A comparison between *in vivo* and *ex vivo* HR-MAS ^{1}H MR spectra of a pediatric posterior fossa lesion

V. TUGNOLI[1], L. SCHENETTI[2], A. MUCCI[2], L. NOCETTI[3], C. TORACI[3], L. MAVILLA[4], G. BASSO[4], R. ROVATI[4], F. TAVANI[4], E. ZUNARELLI[5], V. RIGHI[1,2] and M.R. TOSI[6]

[1]Dipartimento di Biochimica 'G. Moruzzi,' via Belmeloro 8/2, 40126 Bologna; [2]Dipartimento di Chimica, Università di Modena e Reggio Emilia, via G. Campi 183; [3]Struttura Complessa di Fisica Sanitaria and [4]Struttura Complessa di Neuroradiologia, Dipartimento Neuroscienze, Testa e Collo; [5]Struttura Complessa di Anatomia Patologica, Azienda Ospedaliero-Universitaria di Modena - Policlinico, L.go del Pozzo 71, 41100 Modena; [6]ITOI/CNR, Sez. di Bologna, c/o IOR, via di Barbiano 1/10, 40136 Bologna, Italy

Received February 25, 2005; Accepted April 15, 2005

Abstract. The present case report was aimed at identifying the molecular profile characteristic of a primitive neuro-ectodermal tumor (PNET) in a 3-year-old child affected by a lesion localized in the cerebellar region. The histological diagnosis was medulloblastoma. *In vivo* single voxel ^{1}H magnetic resonance spectroscopy (MRS) shows high specificity in detecting the main metabolic alterations in the primitive cerebellar lesion; a very high amount of the choline-containing compounds and very low level of creatine derivatives and N-acetylaspartate. *Ex vivo* high resolution magic angle spinning (HR-MAS) ^{1}H magnetic resonance spectroscopy, performed at 9.4 Tesla on the neoplastic specimen collected during surgery, allows for the unambiguous identification of several metabolites giving a more in-depth evaluation of the metabolic pattern of the lesion. The *ex vivo* HR-MAS MR spectra show that the spectral detail is much higher than that obtained *in vivo* and that, for example, myo-inositol, taurine and phosphorylethanolamine contribute to the *in vivo* signal at 3.2 ppm, usually attributed to choline-containing compounds. In addition, the spectroscopic data appear to correlate with some morphological features of the medulloblastoma. Consequently, the present study shows that *ex vivo* HR-MAS ^{1}H MRS is able to strongly improve the clinical possibility of *in vivo* MRS and can be used in conjunction with *in vivo* spectroscopy for clinical purposes.

Correspondence to: Dr Vitaliano Tugnoli, Dipartimento di Biochimica, Università di Bologna, via Belmeloro 8/2, 40126 Bologna, Italy
E-mail: vitaliano.tugnoli@unibo.it

Professor Adele Mucci, Dipartimento di Chimica, Università di Modena e Reggio Emilia, via G. Campi 183, 41100 Modena, Italy
E-mail: mucci.adele@unimo.it

Dr Gianpaolo Basso, Struttura Complessa di Neuroradiologia, Dipartimento Neuroscienze, Testa e Collo, Azienda Ospedaliero-Universitaria di Modena - Policlinico, L.go del Pozzo 71, 41100 Modena, Italy
E-mail: basso@unimo.it

Key words: in vivo magnetic resonance spectroscopy, *ex vivo* high resolution magic angle spinning magnetic resonance spectroscopy, medulloblastoma, molecular characterization

Introduction

In clinical examinations, *in vivo* magnetic resonance spectroscopy (MRS) is a non-invasive method to detect the biochemical changes accompanying the disease. The clinical impact of MRS in medicine has been widely reviewed by Smith *et al* and shows promise as a method to complement routine diagnostic investigation (1). However, the poor *in vivo* spectral resolution leads to limited characterization of the real biochemical composition of explored tissue. Moreover, even among metabolites that are highly detectable with *in vivo* MRS, subtle concentration differences between normal and pathological tissue, such as a neoplasm, can go unnoticed and result in a diagnostic error.

The detailed biochemical picture of tissue is the basis of correct interpretation by *in vivo* MRS, which can be used when the molecular markers are well established. A deep knowledge of the biochemical composition of tissue can be obtained by spectroscopic analysis on extracts obtained from tissue (*in vitro* MRS) or directly from tissue specimens (*ex vivo* MRS). High resolution magic angle spinning (HR-MAS) *ex vivo* MRS is a powerful analytical tool for human tissue, potentially bridging the divide between *in vitro* and *in vivo* MRS. The first applications of HR-MAS MRS on human tissue specimens date back to 1997 (2,3) and are possible thanks to the commercial diffusion of MRS probe-heads capable of studying samples in rapid rotation around an axis of 54.7° ('magic angle'), tilted with respect to that of the static magnetic field. These probe-heads drastically reduce contributions from dipolar couplings, chemical shift anisotropy and susceptibility

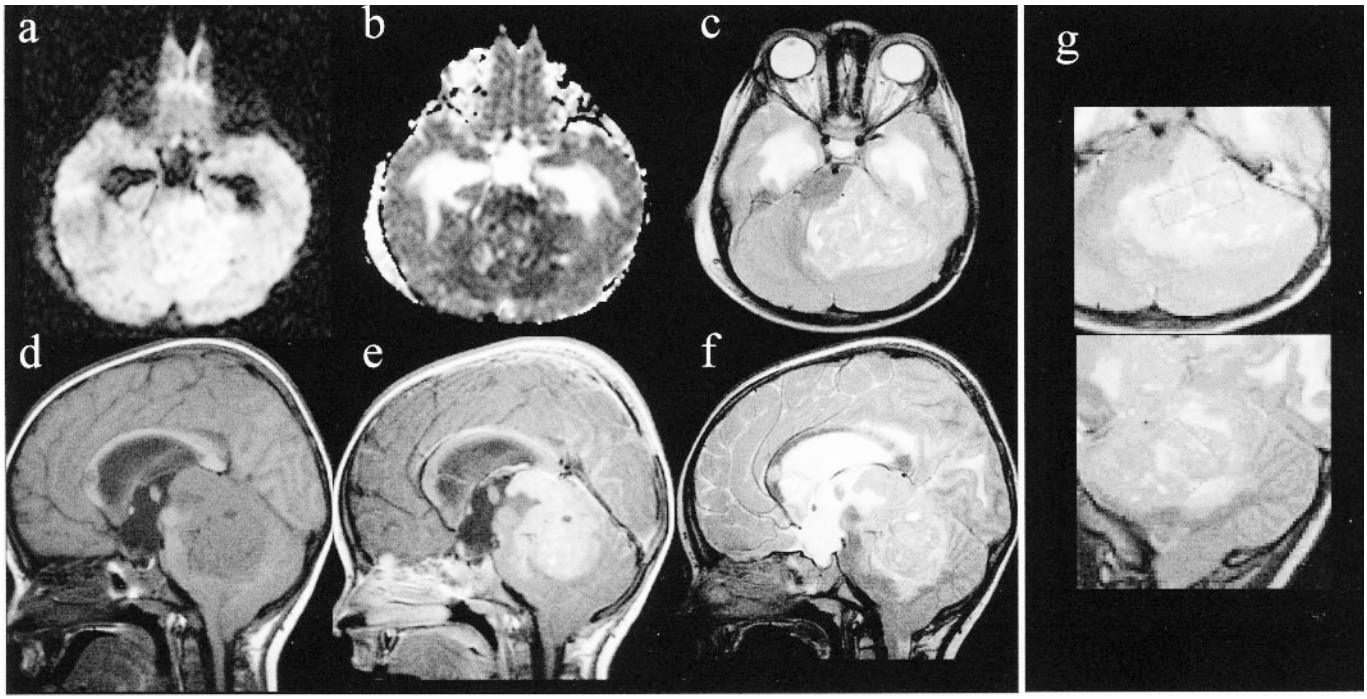

Figure 1. Conventional MR imaging. (a) Axial diffusion weighted; (b) apparent diffusion coefficient; (c) axial T2 weighted; (d) saggital T1 weighted; (e) post-gadolinium sagittal T1 weighted; (f) sagittal T2 weighted; and (g) single voxel localizer displayed in green over T2 weighted axial and sagittal images.

distortions, thus providing high resolution spectra from semi-solid samples such as tissue (4-11). The quality of the obtained spectra is comparable to that obtained from aqueous extracts, and the possible acquisition techniques are the same as those employed in *in vitro* MRS, with the advantage of carrying out measurements on intact tissue specimens without pretreatment.

We present a case where a comparison between *in vivo* single voxel and *ex vivo* HR-MAS ^{1}H MRS was performed on a child affected by medulloblastoma.

Case report

Clinical material. A 3-year-old child was admitted to the hospital because of persistent headaches, which started 1 month previously, and a refusal to eat due to persistent nausea. He underwent magnetic resonance imaging (MRI) and *in vivo* ^{1}H MRS of the head on a 1.5 Tesla clinical imager (Philips Intera, Best, Netherlands), which revealed an intracranial tumor occupying most of the left portion of the posterior fossa. Compared to brain parenchyma, the lesion was predominantly hyperintense on T2-weighted images and slightly hypointense on T1-weighted images with restricted apparent diffusion coefficient (ADC). After intravenous gadolinium injection, the mass was enhanced strongly, but not uniformly due to internal small cystic components (Fig. 1). Extension to supratentorial space through the Pacchioni foramen was clearly visualized, and an extra-axial subarachnoid location was initially suggested. Compression of the fourth and third ventricles and the aqueductus caused marked hypertensive triventricular hydrocephalus. Spine imaging revealed diffused leptomeningeal tumor localizations. The very large dimension of the tumor combined with the high cellular density, as suggested by the restricted ADC, and the apparent extra-axial localization into the subarachnoid space, raised the diagnostic hypotheses of a rare case of lymphoma to be differentiated from medulloblastoma.

After MR examination, a ventricular-peritoneal shunt was positioned. Twelve days after MRI, the child underwent brain surgery, which revealed an intra-axial tumor. Extemporaneous histological examination on a sample was diagnostic for medulloblastoma and extensive, but only partial resection of the tumor was possible.

Subsequent histopathological analysis revealed apoptotic elements, necrosis, high proliferation activity (MIB1 =70%) and highly positive CD56 immunoassay. No nodular aspect was reported.

In vivo ^{1}H MRS. *In vivo* ^{1}H MR spectra were performed using a spin-echo sequence with 144 ms echo time (TE), 2 sec repetition time (TR), and averaging the signal of 128 consecutive scans, 512 data points and PRESS localization technique. Two volumes of interest (VOI) (3x2x2 cm) were placed respectively on the tumor mass (Fig. 1) and on normal-appearing cerebellar parenchyma. Water signal suppression was performed using a standard CHESS sequence with two Gaussian chemical shift selective pulses of 70 Hz. The data were processed using CSX2 (Kennedy Krieger Institute, Baltimore, USA). DC Correction, Zero Filling factor 2, Gaussian Filter with L.B. 3.0 Hz (time domain), High Pass Filter Bandwith 50 Hz (to suppress water peak) and baseline correction was applied to both the spectra data.

Ex vivo HR-MAS ^{1}H MRS. During neurosurgery, a sample of the medulloblastoma was put in liquid nitrogen and stored at -85˚C until *ex vivo* MRS analysis. Before MRS examination,

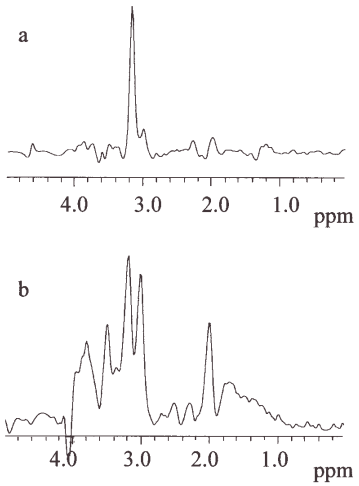

Figure 2. *In vivo* ^{1}H MR spectra of (a) medulloblastoma and (b) contralateral healthy cerebellum.

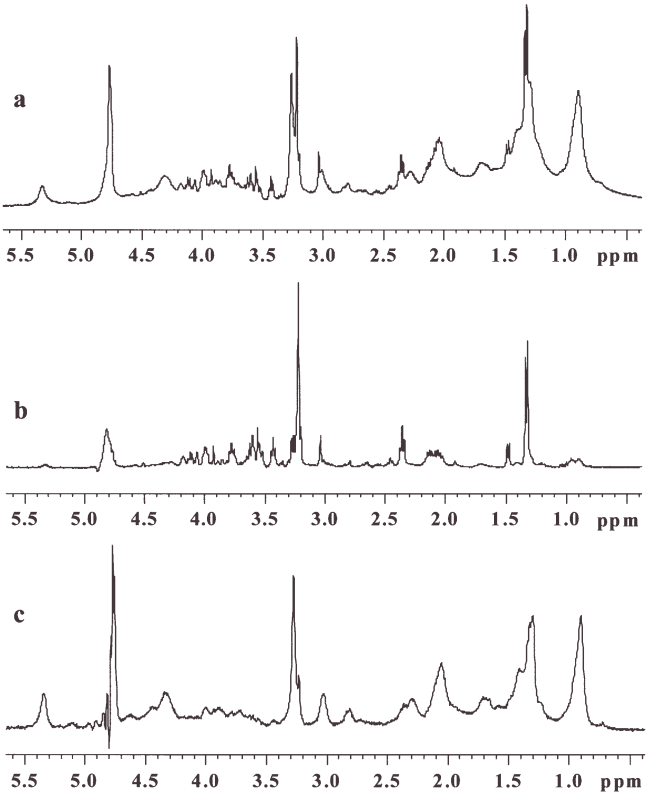

Figure 3. HR-MAS ^{1}H MR spectra of the medulloblastoma. (a) Conventional ^{1}H MR spectrum obtained with water presaturation and composite pulse, (b) CPMG spectrum obtained with 360 ms total spin-echo time and (c) diffusion edited spectrum obtained with Δ =200 ms, δ =4 ms and gradient strength of 32 G/cm.

the sample was flushed with D_2O prior to insertion in the MAS rotor (4 mm OD). Sample and instrument preparation took about 20 min.

Proton HR-MAS spectra were recorded with a Bruker Avance 400 spectrometer equipped with a ^{1}H,^{13}C HR-MAS probe, utilizing the sequences implemented in the Bruker software. The sample was spun at 2800 Hz and three different types of 1D (monodimensional) proton spectra were acquired by using: i) a composite pulse sequence (zgcppr) (12) with 1.5 sec water-presaturation during relaxation delay, 8 kHz spectral width, 32k data points, 32 scans; ii) a water-suppressed spin-echo Carr-Purcell-Meiboom-Gill sequence (cpmgpr) (13) with 1.5 sec water-presaturation during relaxation delay, 1 ms echo time (τ) and 360 ms total spin-spin relaxation delay ($2n\tau$), 8 KHz spectral width, 32k data points, 256 scans; and iii) a sequence for diffusion measurements based on stimulated echo and bipolar-gradient pulses (ledbpgp2s1d) (14) with big delta 200 ms, eddy current delay Te 5 ms, little delta 2x2 ms, sine-shaped gradient with 32 G/cm followed by a 200 μs delay for gradient recovery, 8 kHz spectral width, 8k data points, 256 scans. Two-dimensional ^{1}H,^{1}H-correlation spectroscopy (COSY) (15,16) spectra were acquired using a standard pulse sequence (cosygpprqf) and 0.5 sec water-presaturation during relaxation delay, 8 kHz spectral width, 4k data points, 32 scans per increment, 256 increments. Two-dimensional (2D) ^{1}H,^{1}H-total correlation spectroscopy (TOCSY), (17,18) spectra were acquired using a standard pulse sequence (mlevphpr) and 1 sec water-presaturation during relaxation delay, 100 ms mixing (spin-lock) time, 4 kHz spectral width, 4k data points, 32 scans per increment, 128 increments. Two-dimensional ^{1}H,^{13}C-heteronuclear single quantum coherence (HSQC) (19) were acquired using a echo-antiecho phase sensitive standard pulse sequence (hsqcetgp) and 0.5 sec relaxation delay, 1.725 ms evolution time, 4 kHz spectral width in f_2, 4k data points, 128 scans per increment, 17 kHz spectral width in f_1, 256 increments.

Results and Discussion

The single voxel *in vivo* ^{1}H MR spectra obtained from the medulloblastoma and contralateral healthy cerebellum are reported in Fig. 2a and b, respectively. The spectrum of the lesion (Fig. 2a) displays one predominant signal at 3.2 ppm, which is usually attributed to choline-containing compounds (ChoCC); accompanied by low intensity peaks at 3.0 ppm, attributable to creatine derivatives (Cr); at 2.3 ppm, attributable to glutamate plus glutamine (Glx); and at 2.0 ppm, attributable to *N*-acetylaspartate (NAA) and Glx (5). The high ChoCC/Cr ratio found in the present case can be associated with the synthesis of new cell membranes. Several MRS studies correlate the increase of such compounds to the cell neoplastic proliferation (20,21).

Moreover, it can be noted that signals downfield from ChoCC are nearly absent in the MR spectrum of the lesion with respect to that of the contralateral healthy cerebellum (Fig. 2b). In fact, the *in vivo* MR spectrum of the contralateral VOI shows high signals from NAA at 2.0 ppm, Cr at 3.0 ppm, ChoCC at 3.2 ppm, and myo-inositol (Myo) at 3.5 ppm. Lower signals due to NAA at 2.5 ppm and to Glx at 2.3 ppm are also observed. The signal at 3.5 ppm could receive contributions from both Myo and glycine (Gly). Signals at higher frequencies are poorly resolved. ChoCC/Cr metabolite signal intensity ratio is within the range measured for the cerebellar tissue of healthy children, while a reduction of NAA/ChoCC and NAA/Cr ratios is evident (20-22). We hypothesized that the reduction of NAA was an expression of mild oedema and neuronal dysfunction in the otherwise normal appearing brain tissue chosen for MRS, an effect in agreement with the high compression exerted by the tumor.

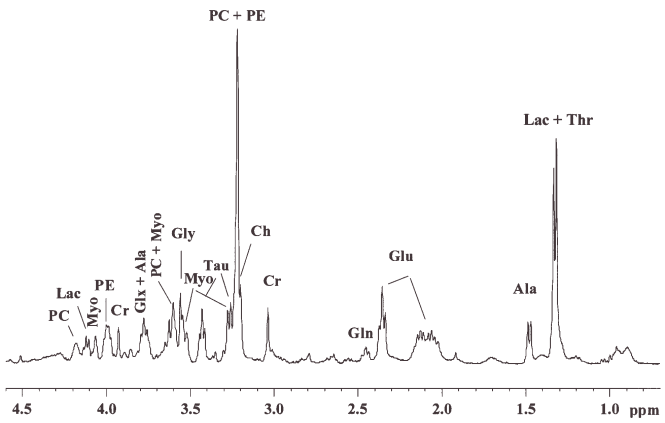

Figure 4. HR-MAS ^{1}H MR spectrum of the medulloblastoma. CPMG spectrum obtained with 360 ms total spin-echo time; the major metabolites are labelled.

Fig. 3 reports the *ex vivo* ^{1}H HR-MAS MR spectra of the medulloblastoma performed with different experiments. A conventional presaturated 1D spectrum, which highlights both lipid and small metabolite contribution, is displayed in panel a. Fig. 3b shows a spectrum obtained using a CPMG spin-echo sequence [90°- $(\tau\text{-}180°\text{-}\tau)_n$], in order to separate signals according to their different T2 and enhance the resonance of metabolites with respect to those of macromolecules. Fig. 3c represents the diffusion-edited spectrum displaying contributions from mobile lipids and macromolecules.

The most abundant metabolites can be assigned by comparison with literature data, but a complete assignment requires the acquisition of selected 2D experiments such as COSY, TOCSY and HSQC. The COSY and TOCSY spectra are very informative for the identification of hidden resonances: the COSY spectra enable the coupled proton-proton pairs to be found, whereas the TOCSY spectra permit the identification of ^{1}H,^{1}H connectivities of up to 5 or 6 bonds. ^{1}H,^{13}C HSQC spectra permit the identification of directly bonded carbon-proton correlations, making it possible to assign singlets (which do not give correlations in homonuclear COSY and TOCSY spectra), and distinguish signals from different molecules having similar proton chemical shifts, but diverse ^{13}C signals. These experiments enable a complete and unambiguous identification of the metabolic pattern characterizing the examined tissue. The principal metabolites are labelled in Fig. 4, and the ^{1}H and ^{13}C assignments of the observed pool of metabolites, particularly osmolites, free amino acids and a fraction of mobile lipids, are reported in Table I.

A look at the HR-MAS spectra shows that the spectral detail is much higher than that obtainable *in vivo,* and that Myo, Tau and phosphorylethanolamine (PE), and a trace of arginine, contribute to the *in vivo* signal at 3.2 ppm, usually attributed to ChoCC [glycerophosphorylcholine (GPC), phosphorylcholine (PC) and free choline (Cho)]. The H-5 proton signal of Myo at 3.28 ppm (triplet) is detected through the correlation with H-4,6 at 3.63 ppm in the COSY spectrum, and the correlations with other protons of its spin system (4.06, 3.63, and 3.53 ppm) in the TOCSY spectrum (Fig. 5a). The CH_2N protons of PE at 3.23 ppm (triplet) are detected in both homonuclear correlation spectra, through a correlation with CH_2O at 4.00 ppm (a double triplet, which resembles a quartet), which shows a coupling with the phosphorous nucleus. Similarly, the CH_2N protons of Tau at 3.26 ppm (triplet) are detected through the correlation with CH_2S at 3.42 ppm (triplet). An estimation of relative contributions of these metabolites to the integral value of signals between 3.32 and 3.15 ppm, usually attributed to the *in vivo* spectra of ChoCC, can be derived from the evaluation of areas of selected

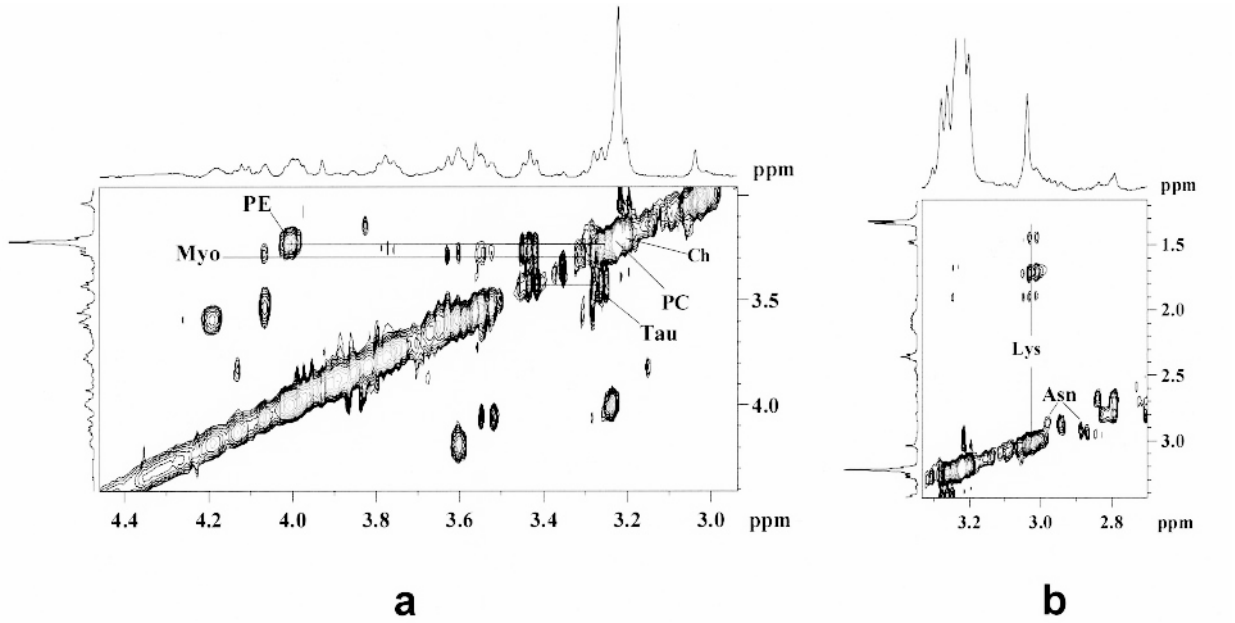

Figure 5. Partial regions of the TOCSY MR spectrum of the medulloblastoma. The identified metabolites are denoted with labels according to Table I.

Table I. List of the ^{1}H and ^{13}C chemical shift (δ, ppm) of metabolites found in HR-MAS MR spectra of the examined medulloblastoma.[a,b]

Metabolite	δ ^{1}H	δ ^{13}C	
Fatty acids	0.89	14.6	CH_3
	1.27-1.33	23.3, 30.5	$(CH_2)_n$
	1.62		CH_2-C-C=O
	2.02		CH_2-C=
	2.29		CH_2C=O
	2.78		=C-CH_2-C=
	5.32	129.6	CH=CH
Isoleucine	0.94(t)		δ-CH_3
	1.02(d)		γ-CH_3
	1.29,1.48		γ-CH_2
	1.97		ß-CH
	3.69		α-CH
Leucine	0.95(d)	21.6	δ-CH_3
	0.97(d)	22.7	δ-CH_3
	1.70	24.8	γ-CH
	1.72		ß-CH_2
	3.75	[c]	α-CH
Valine	0.99(d)	17.3	γ-CH_3
	1.04(d)	18.7	γ-CH_3
	2.25		ß-CH
	3.61		α-CH
Threonine	1.33(d)	20.3	γ-CH_3
	4.27		ß-CH
	3.60		α-CH
Lactate	1.33(d)	20.3	CH_3
	4.11	69.5	CH
Alanine	1.48(d)	16.8	ß-CH_3
	3.79		α-CH
Lysine	3.04	39.9	ε-CH_2
	1.72	27.3	δ-CH_2
	1.48	22.3	γ-CH_2
	1.91	30.6	ß-CH_2
	3.78	[c]	α-CH
Arginine	3.23	41.3	δ-CH_2
	1.69	24.9	γ-CH_2
	1.93	28.3	ß-CH_2
	3.78	[c]	α-CH
Glutamate	2.36(t)	34.3	γ-CH_2
	2.06, 2.15	27.6	ß-CH_2
	3.77	[c]	α-CH
Glutamine	2.48(td)	31.7	γ-CH_2
	2.14		ß-CH_2
	3.79	[c]	α-CH
Proline	3.43,3.34		δ-CH_2
	2.01		γ-CH_2
	2.34,2.07		ß-CH_2
	4.12		α-CH
Aspartic acid	2.68,2.82		ß-CH_2
	3.90		α-CH

Table I. Continued.

Metabolite	δ ^{1}H	δ ^{13}C	
Asparagine	2.85, 2.96		ß-CH_2
	4.01		α-CH
Creatine	3.04(s)	38.0	NCH_3
	3.92(s)	54.8	CH_2
Tyrosine	3.06,3.20		ß-CH_2
	3.93		α-CH
	6.88		H*ortho*
	7.20		H*meta*
Phenylalanine	7.33		H*ortho*
	7.37		H*para*
	7.43		H*meta*
Ethanolamine	3.83		CH_2
	3.15		CH_2
Phosphoryl ethanolamine	3.23 (t)	41.5	CH_2
	4.00 (dt)	61.3	CH_2
Glycerophosphoryl-ethanolamine	3.34		CH_2
	4.13		CH_2
Choline	3.20	54.7	$N(CH_3)_3$
	3.53	68.2	NCH_2
	4.07		OCH_2
Phosphorylcholine	3.22	54.7	$N(CH_3)_3$
	3.61	67.3	NCH_2
	4.19	58.8	OCH_2
Taurine	3.26(t)	48.7	NCH_2
	3.42(t)	36.4	SCH_2
Myoinositol	3.28(t)	75.3	5-CH
	3.63(t)	73.1	4,6-CH
	3.53(dd)	72.3	1,3-CH
	4.06(t)	73.0	2-CH
Scyllo-inositol	3.35 (s)		
Glycine	3.56	42.3	CH_2
UDPG or UMPG	-		5-CH_2rib
	4.13		4-CHrib
	4.23		3-CHrib
	4.36		2-CHrib
	5.92		1-CHrib
	5.91		5-CHur
	7.89		6-CHur
Adenine	8.19		8-CH
	8.23		2-CH
Acetate	1.92		CH_3C=O
Unknown	8.34		

[a]^{1}H chemical shifts are referred to an alanine doublet at 1.48 ppm. [b]^{13}C chemical shifts are referred to alanine at 16.8 ppm. [c]Cα probably contributes to the 3.77, 55.2 ppm cross-peak.

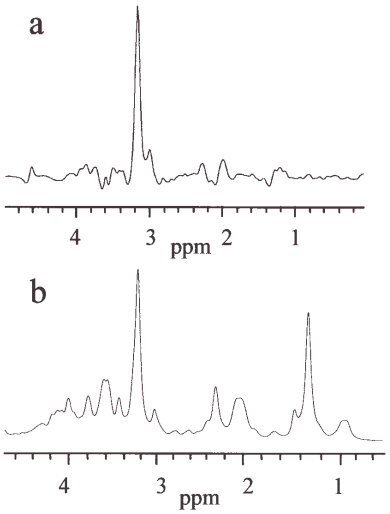

Figure 6. Comparison of the *in vivo* ^{1}H spectrum, recorded at 1.5 T, of the medulloblastoma (a) and its *ex vivo* ^{1}H HR-MAS spectrum, recorded at 9.4 Tesla (b); an exponential function with a 30-Hz line broadening (LB) was applied prior to the Fourier transformation with the aim of having a spectrum line width comparable to the *in vivo* spectrum.

signals (weighted on the basis of the relative proton numbers). This calculation leads to the presence of 20% PE, 18% Tau, 55% PC + Cho, and 7% Myo. The same experiments highlight a contribution from the CH_2N lysine and CH_2COO^- asparagine signals to the *in vivo* signal at 3.0 ppm, usually attributed to NCH_3 creatine protons (Fig. 5b). Creatine participates in 60% of the total area of the region 3.10-2.90 ppm, as deduced by comparison of the integral of the signal at 3.92 ppm (CH_2 protons of creatine).

Finally, *ex vivo* ^{1}H MRS experiments indicate the presence of alanine (Ala) and lactate (Lac) and the absence of NAA. The absence of NAA in the HR-MAS spectra and presence of only a trace of acetate suggest that the peak at 2.0 ppm in the *in vivo* spectrum could be principally due to the CH_2(ß) and CH_2(γ) signals of glutamate plus glutamine.

A direct comparison between the *in vivo* and *ex vivo* MR profiles of medulloblastoma can be made after applying a broadening processing function to the HR-MAS signal which, although implying the loss of a higher degree of information furnished by the HR-MAS spectrum, shows the close correspondence between the two spectra (Fig. 6), especially when the region of ChoCC and Cr signals is considered. The highest signal is that usually attributed to ChoCC, which we have shown above to receive contributions from a number of other metabolites, accompanied by low intensity peaks due to glutamate plus glutamine at 2.3 and 2.0 ppm, and Cr (plus lysine and asparagine) at 3.0 ppm. More difficult is the comparison between regions at higher frequencies of the two spectra, where signals due to Tau, Myo, Gly and PE are expected. These signals are evident in the *ex vivo* spectrum, but they are less clear *in vivo* because of more distortions from the evolution of coupling constants. The estimation of the ratio ChoCC/Cr from the *in vivo* spectrum (5/1) compares well with that from the HR-MAS spectrum (6.5/1) obtained, considering the regions 3.15-3.32 and 3.10-2.90 ppm. Myo, Tau, Gly and PE have already been reported as significant metabolites from *in vitro* MRS studies on medulloblastoma (25,26). Accordingly, prominent Tau, Gly and PE peaks are easily observed in our *ex vivo* spectrum (Fig. 4), and the presence of Tau in *in vivo* spectra of the medulloblastoma has been reported (27,28).

Further considerations can be argued from the analysis of *ex vivo* MR spectra. Mobile lipids, which are already visible in the standard presaturated 1D spectrum (Fig. 3a), are further evidenced in the diffusion-edited spectrum (Fig. 3c) by the broad signals at 0.89, 1.30, 3.26 and 5.32 ppm. In particular, the 3.26 ppm resonance, deriving from the trimethylammonium of the choline residue, strongly suggests that phospholipids are present in substantial amounts in the examined medulloblastoma. It is worthwhile to underline the presence of broad signals at 3.02 and 1.72 ppm (which are correlated by the TOCSY experiments also to the 1.48 and 1.91 ppm signals), attributable to lysine in non-negligible amounts and possibly involved in lysyl-phosphatidylglycerols. These findings provide a deeper insight into the lipid composition of brain neoplasms to be pursued. It has been reported that the presence of mobile lipids, both in *ex vivo* and *in vivo* MR spectra of brain neoplasms, is correlated to necrosis in the lesions (29,30). This spectroscopic datum directly correlates to a morphological aspect of the histopathological assessment. Moreover, Tzika *et al* reported that *in vivo* and *ex vivo* MR spectra of several pediatric brain tumors exhibited substantial levels of lipids, which may be due to apoptosis and/or necrosis (31). As a consequence, the histological features of apoptosis and necrosis, evidenced in the histological analysis of this medulloblastoma, are reflected by the presence of lipid signals in our *ex vivo* HR-MAS MR spectra.

In this case report, we have demonstrated that the *ex vivo* HR-MAS MR spectroscopy can reach a high resolution degree, thus providing a link between *in vivo* MRS and neuropathological analysis. The present study demonstrates that *ex vivo* HR-MAS ^{1}H MRS is able to strongly improve the clinical possibility of *in vivo* MRS and can be used in conjunction with *in vivo* spectroscopy for clinical purposes, in which case a large number of samples can be analyzed and histologically classified.

Acknowledgements

The Fondazione Cassa di Risparmio di Modena is greatly acknowledged for financial support, which assisted in the acquisition of the Bruker Avance 400 Spectrometer and Philips Intera 1.5 Tesla MR scanner. The Centro Interdipartimentale Grandi Strumenti of the University of Modena and Reggio Emilia and the Azienda Ospedaliero-Universitaria Policlinico di Modena are also greatly acknowledged for providing the use of their facilities. This work was supported by grants from Murst ex 60% to V.T.

References

1. Smith ICP and Stewart LC: Magnetic resonance spectroscopy in medicine: clinical impact. Prog Nuclear Magn Reson Spectroscopy 40: 1-34, 2002.
2. Millis KK, Maas WE, Cory DG and Singer S: Gradient, high-resolution, magic-angle spinning nuclear magnetic resonance spectroscopy of human adipocyte tissue. Magn Reson Med 38: 399-403, 1997.

3. Cheng LL, Ma MJ, Becerra L, Ptak T, Tracey I, Lackner A and Gonzalez RG: Quantitative neuropathology by high resolution magic angle spinning proton magnetic resonance spectroscopy. Proc Natl Acad Sci USA 94: 6408-6413, 1997.
4. Millis K, Weybright P, Campbell N, Fletcher JA, Fletcher CD, Cory DG and Singer S: Classification of human liposarcoma and lipoma using *ex vivo* proton NMR spectroscopy. Magn Reson Med 41: 257-267, 1999.
5. Barton SJ, Howe FA, Tomlins AM, Nicholson JK, *et al*: Comparison of *in vivo* ^{1}H MRS of human brain tumors with ^{1}H HR MAS spectroscopy of intact biopsy samples *in vitro*. Magn Res Mat Phys Biol Med (MAGMA) 8: 121-128, 1999.
6. Garrod S, Humpfer E, Spraul M, *et al*: High-resolution magic angle spinning ^{1}H NMR spectroscopic studies on intact rat renal cortex and medulla. Magn Res Med 41: 1108-1118, 1999.
7. Tate AR, Foxall PJD, Holmes E, *et al*: Distinction between normal and renal carcinoma kidney cortical biopsy samples using pattern recognition of ^{1}H magic angle spinning (MAS) NMR spectra. NMR Biomed 13: 64-71, 2000.
8. Sitter B, Sonnewald U, Spraul M, *et al*: High-resolution magic angle spinning MRS of breast cancer tissue. NMR Biomed 15: 327-337, 2002.
9. Taylor JL, Wu CL, Cory D, Gonzalez RG, Bielecki A and Cheng LL: High-resolution magic angle spinning proton NMR analysis of human prostate tissue with slow spinning rates. Magn Reson Med 50: 627-633, 2003.
10. Wang Y, Bollard ME, Keun H, *et al*: Spectral editing and pattern recognition methods applied to high-resolution magic-angle spinning ^{1}H nuclear magnetic resonance spectroscopy of liver tissues. Anal Biochem 323: 26-32, 2003.
11. Swanson MG, Vigneron DB, Tabtabai L, *et al*: Proton HR MAS spectroscopy and quantitative pathologic analysis of MRI/3D-MRSI-targeted postsurgical prostate tissues. Magn Res Med 50: 944-954, 2003.
12. Bax A: A spatially selective composite 90˚ radiofrequency pulse. J Magn Reson 65: 142-145, 1985.
13. Meiboom S and Gill D: Modified spin-echo method for measuring nuclear relaxation time. Rev Sci Instrum 20: 688-691, 1958.
14. Wu D, Chen A and Johnson CS Jr: An improved diffusion-ordered spectroscopy experiment incorporating bipolar gradient pulses. Magn Reson Series A 115: 260-264, 1995.
15. Jeener J: Pulse pair techniques in high resolution NMR. Ampere International Summer School II, Basko Polje, 1971.
16. Aue WP, Bartholdi E and Ernst RR: Two-dimensional spectroscopy. Application to nuclear magnetic resonance. J Chem Phys 64: 2229-2246, 1976.
17. Braunschweiler L and Ernst RR: Coherence transfer by isotropic mixing: application to proton correlation spectroscopy. J Magn Reson 53: 521-528, 1983.
18. Bax A and Davis DG: MLEV-17-based two-dimensional homonuclear magnetization transfer spectroscopy. J Magn Res 65: 355-360, 1985.
19. Bodenhausen G and Ruben DJ: Natural abundance nitrogen-15 NMR by enhanced eteronuclear spectroscopy. Chem Phys Lett 69: 185-189, 1980.
20. Barbarella G, Ricci R, Pirini G, Tugnoli V, Tosi MR, *et al*: *In vivo* single voxel ^{1}H MRS of glial brain tumors: correlation with tissue histology and *in vitro* MRS. Int J Oncol 12: 461-468, 1998.
21. Shimizu H, Kumabe T and Yoshimoto T: Correlation between Choline level measured by proton MR spectroscopy and Ki-67 labeling in gliomas. AJNR Am Neuroradial 21: 659-665, 2000.
22. Wang Z, Sutton L, Cnaan A, Haselgrove JC, Rorke LB, *et al*: Proton MR spectroscopy of pediatric cerebellar tumors. AJNR Am J Neuroradiol 16: 1821-1833, 1995.
23. Tedeschi G, Bertolino A, Righini A, Campbell G, Raman R, *et al*: Brain regional distribution pattern of metabolite signal intensities in young adults by proton magnetic resonance spectroscopic imaging. Neurology 45: 1384-1391, 1995.
24. van der Knaap MS, van der Grond J, van Rijen PC, Faber JA, Valk J and Willemse K: Age-dependent changes in localized proton and phosphorus MR spectroscopy of the brain. Radiology 176: 509-515, 1990.
25. Kinoshita Y and Yokota A: Absolute concentrations of metabolites in human brain tumors using *in vitro* proton magnetic resonance spectroscopy. NMR Biomed 10: 2-12, 1997.
26. Sutton LN, Wehrli SL, Gennarelli L, *et al*: High-resolution ^{1}H-magnetic resonance spectroscopy of pediatric posterior fossa tumors *in vitro*. J Neurosurg 81: 443-448, 1994.
27. Wilke M, Eidenschink A, Muller-Weihrich S and Auer DP: MR diffusion imaging and ^{1}H spectroscopy of a child with medulloblastoma. A case report. Acta Radiology 42: 39-42, 2001.
28 Moreno-Torres A, Martinez-Perez I, Baquero M, *et al*: Taurine detection by proton magnetic resonance spectroscopy in medulloblastoma: contribution to noninvasive differential diagnosis with cerebellar astrocytoma. Neurosurgery 55: 824-829, 2004.
29. Kusel AC, Donnelly SM, Halliday W, Sutherland GR and Smith IC: Mobile lipids and metabolic heterogeneity of brain tumors as detected by *ex vivo* ^{1}H MR spectroscopy. NMR Biomed 7: 172-180, 1994.
30. Negendank W and Sauter R: Intratumoral lipids in ^{1}H MRS *in vivo* in brain tumors: experience of Siemens cooperative clinical trial. Anticancer Res 16: 1533-1538, 1996.
31. Tzika AA, Ling Cheng L, Goumnerova L, Madsen JR, Zurakowski D, *et al*: Biochemical characterization of pediatric brain tumors by using *in vivo* and *ex vivo* magnetic resonance spectroscopy. J Neurosurg 96: 1023-1031, 2002.